Polyhedron 173 (2019) 114116

Contents lists available at ScienceDirect

Polyhedron

journal homepage: www.elsevier.com/locate/poly

Synthesis, crystallographic studies, molecular modeling and *in vitro* biological studies of silver(I) complexes with aminoadamantane ligands

Anna Karla dos Santos Pereira [a,*], Douglas Hideki Nakahata [a], Carlos Marrote Manzano [a], Déborah de Alencar Simoni [a], Douglas Henrique Pereira [b], Wilton Rogério Lustri [c], André Luiz Barboza Formiga [a], Pedro Paulo Corbi [a,*]

[a] Institute of Chemistry, University of Campinas – UNICAMP, PO Box 6154, 13083-970 Campinas, SP, Brazil
[b] Chemistry Collegiate, Federal University of Tocantins, Campus Gurupi, PO Box 66, Gurupi 77 402-970, Brazil
[c] Department of Biological and Health Sciences, University of Araraquara, UNIARA, 14801-320 São Paulo, Brazil

ARTICLE INFO

Article history:
Received 7 May 2019
Accepted 15 August 2019
Available online 23 August 2019

Keywords:
Silver
Amantadine
Memantine
DFT studies
Antibacterial agents

ABSTRACT

Silver(I) complexes with amantadine (atd) and memantine (mtn) were synthesized and characterized. Elemental, thermogravimetric and mass spectrometric analyses indicated a 1:2 metal/ligand ratio, with the molecular composition $AgC_{20}H_{34}N_2{\cdot}NO_3$ for Ag–atd and $AgC_{24}H_{42}N_2{\cdot}NO_3{\cdot}H_2O$ for Ag–mtn. The crystal structures of the silver(I) complexes were determined by single crystal X-ray diffractometric studies and show the coordination of amantadine and memantine to the Ag(I) ion by the nitrogen atom of the NH_2 group. The spectral analysis by infrared and ^1H, ^{13}C and $\{^{15}N,^1H\}$ nuclear magnetic resonance (NMR) spectroscopies confirmed the coordination sites of the ligands to the silver ions. Computational studies revealed modes of vibration and bond lengths similar to those found experimentally. The *in vitro* antibacterial activity assays showed that amantadine is not active over the tested strains while memantine showed a low activity against *Staphylococcus aureus* and *Pseudomonas aeruginosa*. On the other hand, the complexes had a pronounced antibacterial activity over the same strains with minimum inhibitory concentration (MIC) values in the micromolar range. Biophysical assays based on fluorescence spectroscopy indicated that the silver(I) complexes interact weakly with bovine serum albumin, while agarose gel electrophoresis and competitive binding experiments revealed that the compounds interact with DNA by non-covalent interactions.

1. Introduction

Silver compounds have been explored as antimicrobial agents for centuries. After the first reports of the antibacterial activities of silver sulfadiazine (SSD), used in the treatment of bacterial infections in burn wounds in the 1960s, the interest in the synthesis of new silver-based compounds increased considerably [1]. In addition to their antibacterial activities, silver compounds have also been reported for their antifungal [2], antiproliferative [3] and antiviral [4,5] properties.

The mechanism of antimicrobial activity of Ag(I) is related to its possible interaction with nucleic acids or interaction with the cell membrane by reaction with thiol groups of proteins [6,7]. However, the choice of the ligand is determinant for the success of a new silver complex as a metallodrug. It has been observed that the ligand can play an important role in the properties of the compounds including stability, solubility and release of silver ions [6].

Due to the growth of the multiresistant bacterial strains, new approaches have been applied to the development of new and improved antibacterial agents. One of the strategies to overcome the resistance of microorganisms to the antibacterial agents is to combine bioactive ligands and metals with already known antimicrobial activities as copper, silver and gold [8–10].

Abbreviations: atdH, amantadine hydrochloride; atd, amantadine; mtnH, memantine hydrochloride; mtn, memantine; Ag–atd, silver(I) complex with amantadine; Ag–mtn, silver(I) complex with memantine; ATCC, American type collection cell; BSA, bovine serum albumin; DFT, Density Functional Theory; DMSO, dimethylsulfoxide; DNA, deoxyribonucleic acid; ESI(+)-QTOF-MS, electrospray ionization quadrupole time-of-flight mass spectrometry; HMBC, heteronuclear multiple bond coherence; IR, infrared; LANL2DZ, Los Alamos National Laboratory, 2nd version on double zeta function; MIC, minimum inhibitory concentration; NMR, nuclear magnetic resonance; PES, potential energy surface; SSD, silver sulfadiazine; SYBR Green, Nucleic acid electrophoresis stain: N′,N′-dimethyl-N-[4-[(E)-(3-methyl-1,3-benzothiazol-2-ylidene)methyl]-1-phenylquinolin-1-ium-2-yl]-N-propylpropane-1,3-diamine.

* Corresponding authors.
E-mail addresses: a209764@dac.unicamp.br (A.K. dos Santos Pereira), ppcorbi@unicamp.br (P.P. Corbi).

https://doi.org/10.1016/j.poly.2019.114116
0277-5387/

Amantadine (1-aminoadamantane, Fig. 1a) is known for its action against the replication of the *influenza A* virus. The mechanism of inhibition of viral replication is related with the direct interaction of the drug with the ion channel of the M2 viral protein, interrupting the protonation step, and also indirectly with the pH-dependent conformational change of hemagglutinin (HA) [11,12].

Memantine (1-amino-3,5-dimethyladamantane, Fig. 1b), on the other hand, is the dimethyl derivative of amantadine which was approved in 2002 as a drug for the treatment of severe and moderate cases of Alzheimer's disease by the European Agency for the Evaluation of Medical Products (EMEA) [13] and one year later by Food and Drug Administration (FDA) [14]. This drug was also evaluated against subtypes *influenza A* virus and, at high concentrations, presented interference in the viral replication by affecting the fusion activity of the HA only [11].

When a single point mutation happens in the genetic sequence encoding for specific amino acids of the M2 protein, there is virus resistance to amantadine [11,15]. Li et al. [16] reported the effects of silver nanoparticles (AgNPS) functionalized with neutral amantadine (atd) and verified that AgNPS-atd disrupted the morphology of the H1N1 virus after 30 min of interaction and also increased the cell viability from 39% to 90%, presenting better activity when compared to its isolated constituents.

Jimenez et al. [17] synthesized two new silver complexes with ligands derived from adamantylamines with improved aqueous solubility and verified the antibacterial potential of the compounds against Gram-negative and Gram-positive bacterial strains. The authors found that one of the prepared complexes, named $[Ag(qyTAm)_2](CF_3SO_3)$] (where qyTAm = 2-(quinonyl) iminotriazaadamantane), releases Ag(I) ions and presents MIC values comparable to $AgNO_3$ and SSD. The first results about the synthesis of a silver(I) complex with amantadine of composition $Ag(1\text{-}AdNH_2)_2{\cdot}NO_3{\cdot}0.5CH_3OH$ were recently published in the literature [18]. In that case, the composition of the complex was evaluated by elemental analysis, while the coordination of the ligand to the metal ion was suggested by infrared and ^1H and ^{13}C NMR data. No structural determination has been reported so far.

Herein, we describe the synthesis, single crystal X-ray structural determination, ^1H, ^{13}C and $\{^{15}N,^1H\}$ correlation NMR data and electrospray ionization quadrupole time-of-flight mass spectrometric studies (ESI-QTOF-MS) of the silver(I) complex with amantadine and of a new silver(I) complex with memantine. A correlation between theoretical (DFT) and experimental data and complementary studies about the biological activities of the complexes, including interaction with biomolecules, are also presented in this manuscript.

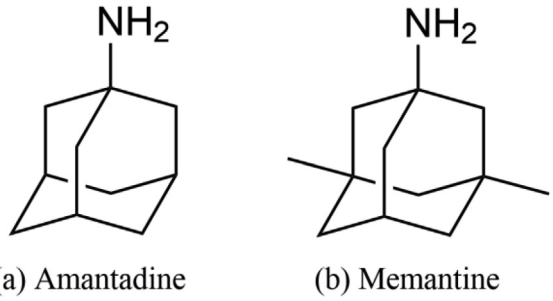

Fig. 1. Molecular structures of (a) amantadine and (b) memantine.

2. 2. Experimental

2.1. Materials and methods

All reagents were of commercial grade and used without further purification. Amantadine hydrochloride (atdH) was obtained from Merck and memantine hydrochloride (mtnH) obtained from Acros Organics. Bovine serum albumin (BSA), silver nitrate ($AgNO_3$), SYBR Green and cisplatin were purchased from Sigma-Aldrich laboratories. Deoxyribonucleic acid (DNA) Ladder 1Kb Plus was purchased form Invitrogen. Elemental analyses for carbon, hydrogen and nitrogen were performed using a Perkin-Elmer CHNS/O Analyzer Model 2400. Infrared (IR) spectra were measured in an Agilent Cary 630 FTIR spectrometer, using the Attenuated Total Reflectance (ATR) method, in the range 4000–400 cm^{-1} and with resolution of 4 cm^{-1}. Thermogravimetric (TG) and differential thermal analyses (DTA) were performed on a simultaneous TGA/DTA SEIKO EXSTAR 6000 thermoanalyzer in the following conditions: synthetic air, flow rate of 100 mL min^{-1} and heating rate of 10 °C min^{-1}, from 25 °C to 900 °C for the silver complex with amantadine. For the silver complex with memantine, the heating rate was of 20 °C min^{-1} and the temperature range was 25–1000 °C. Solution-state nuclear magnetic resonance (NMR) spectra for the ligand and complexes were recorded on Bruker AVANCE III 400 and 500 MHz spectrometers. The NMR spectra were acquired in deuterated dimethylsulfoxide (DMSO-d_6) solutions. Electrospray ionization quadrupole time-of-flight mass spectrometric (ESI(+)-QTOF-MS) measurements were carried out in a Waters Xevo Q-Tof instrument. Samples of the complexes were dissolved in a H_2O/methanol 50:50 solution with 0.1% of formic acid and diluted to the appropriate concentration. The resulting solution was directly infused into the instrument's ESI source. The fluorescence spectra were obtained in a Cary Eclipse fluorescence spectrophotometer, with the use of a quartz cuvette of four clear windows and optical path length of 1.0 cm. The scanning speed was set to slow (BSA) and medium (DNA) and excitation and emission slits set to 5 and 10 nm, respectively.

2.2. Isolation of amantadine and memantine in neutral forms

Initially, its was necessary to neutralize atdH and mtnH and thus eliminate the chloride ions to avoid interference in the synthesis of the silver complexes. So, 2.0 mmol of atdH (375.4 mg) were dissolved in 24 mL of H_2O and the solution was treated with 16.0 mL of a 5% aqueous solution of sodium hydroxide (NaOH) and 1.3 g of sodium chloride (NaCl). The reaction mixture was submitted to extraction (4×) with 10.0 mL of dichloromethane (CH_2Cl_2). A portion of anhydrous sodium carbonate (Na_2CO_3) was added to the organic fraction to remove water and filtered afterwards. The solvent was removed in a rotary evaporator. Yield 94% (284.3 mg). The same process was performed for mtnH, but adjusted for 1.14 mmol (245 mg). Yield 56.8% (116.2 mg).

2.3. Synthesis of Ag–atd complex

Free amantadine (0.90 mmol) was first dissolved in a solution containing 5.0 mL of water and 1.0 mL of a 1.25 mol L^{-1} aqueous solution of nitric acid (HNO_3). After one hour of stirring at room temperature, an aqueous solution containing 0.90 mmol of silver nitrate was added to the solution of the ligand (molar composition 1:1 metal/ligand). Then, a solution of potassium hydroxide (0.44 mol L^{-1}) was added dropwise to the reaction mixture, with precipitation of a light-gray solid. The solid obtained was collected by filtration, washed with water and dried in a desiccator over P_4O_{10}. Yield 38% (161.5 mg). Calcd for $C_{20}H_{34}AgN_3O_3$ (%): C, 50.9;

H, 7.20; N, 8.89. Found (%): C, 50.1; H, 7.17; N, 8.85. Single crystals suitable for diffraction studies were obtained by slow evaporation of an ethanol solution of the silver complex. Although the experimental percentage of carbon for the Ag–atd complex is higher than 0.4% when compared to the calculated value, the experimental hydrogen and nitrogen values are in agreement with the expected ones for the composition suggested. Additional analyses presented in the sequence of manuscript corroborate the suggested composition for this complex.

2.4. Synthesis of Ag–mtn complex

Similar to the Ag–atd synthesis, free memantine (0.52 mmol) was dissolved in a solution containing 5.0 of water and 1.0 mL of a 1.25 mol L^{-1} aqueous solution of HNO_3. The reaction mixture was kept under stirring with fast heating (~55 °C) until complete solubility. Then, an aqueous solution containing 0.26 mmol of silver nitrate was added to the solution of the ligand (molar composition 1:2 metal/ligand) and pH adjusted with addition dropwise of solution KOH (0.44 mol L^{-1}). There was precipitation of a light-gray solid. The solid obtained was collected by filtration, washed with water and dried in a desiccator over P_4O_{10}. Yield 39% (112.3 mg). Calcd for $C_{24}H_{42}AgN_3O_3{\cdot}H_2O$ (%): C, 52.7; H, 8.05; N, 7.68. Found (%): C, 53.1; H, 8.21; N, 7.67. Single crystals suitable for diffraction studies were obtained by slow evaporation of an acetone solution of the silver complex.

2.5. Structural analysis of Ag–atd and Ag–mtn by single-crystal X-ray diffraction data

Data collection for the single-crystals of Ag–atd and Ag–mtn were performed with a Bruker Apex II CCD diffractometer with graphite monochromated Mo Kα (λ = 0.71703 Å) radiation. Unit cell dimensions and orientation matrices were determined by least squares refinement of the reflections obtained by *phi* and *omega* scans. The data were indexed and scaled with the Bruker Apex2 Suite. The structures were solved with the SHELXT [19] structure solution program using intrinsic phasing and refined with SHELXL [20] in OLEX2 (v. 1.2.10) [21]. All nonhydrogen atoms were refined anisotropically and hydrogen atoms were added to the structure in idealized positions and refined according to the riding model with C—H = 0.99 Å and U_{iso}(H) = 1.2 U_{eq}(C) and N—H = 0.91 Å and U_{iso}(H) = 1.2 U_{eq}(N). The disorder on the nitrate counter-ion across a symmetry element in Ag–atd (occupancy set to 0.5) was treated accordingly. Disordered water molecules were included in the refinement of the Ag–mtn crystal, but their corresponding hydrogen atoms were not found in the residual density map and were not added to the final model. Additionally, the Flack parameter found in the refinement of Ag–mtn deviates from zero because of the racemic nature of the sample. Molecular graphics were generated using Olex2 and Mercury [22]. Searches on the Cambridge Structural Database (CSD, v. 5.39) [23] were performed in ConQuest (v. 1.23) [24]. Crystallographic information of Ag–atd and Ag–mtn can be found at the Supplementary Material, Table S1.

2.6. Computational simulations

Theoretical calculations of the compounds were performed using the Density Functional Theory (DFT) with the hybrid functional WB97XD [25]. The 6-31+G(d,p) [26–28] basis set was used for amantadine and memantine and LANL2DZ [29] effective core potential basis set was used for the silver atom. To confirm that the optimized structures were at their minimum energy, frequency calculations were employed and no imaginary frequency was found. To correct the error associated with the harmonic frequencies related to the method, the scale factor 0.952 was used. All calculations were performed using the GAUSSIAN 09 program [30].

2.7. Minimum inhibitory concentration (MIC) assay

The minimum inhibitory concentration values (MIC) were obtained following the methodology described in the literature [31]. For this assay, stock solutions of the samples Ag–atd, Ag–mtn, atdH, mtnH and $AgNO_3$ in DMSO 20% (10 mg mL^{-1}) were prepared prior to serial dilution and Gram-positive (*Staphylococcus aureus* ATCC 25923 and *Bacillus cereus* ATCC 14579) and Gram-negative (*Escherichia coli* ATCC 25922 and *Pseudomonas aeruginosa* ATCC 27583) bacterial strains were inoculated in tubes containing 10.0 mL of Brain Heart Infusion KASVI (BHI) and incubated for 18 h at 35–37 °C. An enough inoculum from each bacterial suspension was added in new tubes containing sterile BHI and incubated at 35–37 °C until the turbidity equaled 1.0 McFarland scale (~3.0×10^8 CFU mL^{-1}). A volume of 30 μL of the samples suspended in 20% aqueous DMSO solution were added to the second well of the 96-well microplate. A volume of 30 μL of the samples suspended in 20% aqueous DMSO solution were added to the second well of the 96-well microplate. Subsequently, serial dilutions of the compounds were performed in 20% aqueous DMSO solution. Then, 70 μL of sterile BHI medium were added to all wells of the microplate. Afterwards, 100 μL of the bacterial suspensions were added in serial dilutions, reaching a 0.5 McFarland scale (~1.5×10^8 CFU mL^{-1}) in a final volume of 200 μL/well, with the concentrations of the compounds varying from 2000 μg mL^{-1} to 0.48 μg mL^{-1}. The final concentration of DMSO in each well of the microplate corresponds to 3% in the total volume of 200 μL/well. Ampicillin (Sigma) was used as positive control with concentrations varying from 10.000 μg mL^{-1} to 0.156 μg mL^{-1}. The microplate was incubated for 18 h at 35–37 °C in a humidity chamber under stirring at 100 rpm. After the incubation period, 15 μL of resazurin at 0.02% were added to each well and after 4 h of reincubation the results were analyzed. The first well was used as positive growth control by the addition of 70 μL of BHI, 30 μL of a solution of DMSO 20% and 100 μL of the bacterial suspension on 1.0 McFarland scale.

2.8. Agarose gel electrophoresis

The compounds Ag–atd, Ag–mtn, atdH, mtnH, $AgNO_3$ and cisplatin were dissolved in DMSO and diluted to 250 μmol L^{-1} in phosphate buffer ($HPO_4^{2-}/H_2PO_4^-$, pH = 7.4). Different amounts of each sample were added to 15 μL pGEX-4T1 plasmid DNA solution to a final concentration of 70 μmol L^{-1} or 35 μmol L^{-1} of compound in phosphate buffer solution and incubated at 37 °C for one hour. Then, 5 μL of the loading buffer (bromophenol blue 0.25% m/v, xylene cyanol 0.25% m/v, glycerol 30% m/v and EDTA 30 mmol L^{-1} in sterile distilled water) were added to each sample. The agarose gel matrix (0.8%) was prepared in Tris–Borate–EDTA 0.5× buffer at pH 8.3 and submitted to electrophoresis for 2.5 hours at 100 V in a BIO-RAD electrophoresis system (Sub-Cell GT cell and PowerPac Basic power supply). The control used was pure pGEX-4T1 plasmid and DNA Ladder 1Kb Plus (12000 bp) was used as weight marker. After electrophoresis, the gel was stained with 1× SYBR Green solution for 3 h and photodocumented using a UVDoc 400i Delpho equipment.

2.9. Probing DNA interaction by fluorescence spectroscopy

Samples of CT-DNA at 100 μmol L^{-1} (in phosphate buffer 10 mmol L^{-1} and 1.5% DMSO) were incubated for 20 h at 37 °C with atdH, mtnH, Ag–atd and Ag–mtn in ratio [compound]/[DNA] of 0.3 (30 μmol L^{-1}). SYBR Green I® (SG) was used as a fluorescent

probe. Excitation wavelength was set as 485 nm and emission window from 505 to 600 nm. For each sample the fluorescence at 520 nm was monitored with the consecutive addition of 4 μL of SG 5×. Measurements were performed in triplicate.

2.10. Probing BSA interaction by fluorescence spectroscopy

Samples of bovine serum albumin (BSA, MW 66 463 Da, extinction coefficient 43 824 M^{-1} cm^{-1} at 279 nm) at concentration of 2.6 μmol L^{-1} were prepared in phosphate buffer solution (HPO_4^{2-}/$H_2PO_4^-$, 50 mmol L^{-1}, pH 7.3) and titrated at 25 °C with solutions of Ag–atd, Ag–mtn, atdH, mtnH and $AgNO_3$ in DMSO to ensure solubilization. In the titration, 2.5 μL of sample solution were added successively to the BSA solution to obtain concentrations of 5.0–30.0 μmol L^{-1} of quencher. Fluorescence emission of BSA was monitored from 300 to 450 nm (excitation at λ = 280 nm) at 25 °C. The results were treated according to the Stern–Volmer equation for quantitative analysis of the fluorescence-quenching data.

$$\frac{F_0}{F} = 1 + K_{SV} \cdot [Q] = 1 + K_q \cdot \tau_0 \cdot [Q]$$

where F_0 is the intensity of fluorescence in the absence of the quencher, F is the intensity of fluorescence in the presence of the quencher, K_{sv} is the Stern–Volmer constant, [Q] is the concentration of the quencher, K_q is the biomolecular quenching rate constant and τ_0 is the average lifetime of the fluorophore in the absence of the quencher (approximately 10^{-9} s for BSA) [32]. The value of K_{sv} is equivalent to the slope of the line equation obtained by the linear regression of the plot F_0/F versus [Q].

Changes in fluorescence intensity caused by the presence of the complex suggest possible complex–protein interactions. The determination of the binding constant (K_b) is valued by the Scatchard equation [33]:

$$log\frac{F_0 - F}{F} = \log[K_b] + n.\log[Q]$$

The value of K_b and n corresponds to the intercept and slope, respectively, of the line equation obtained by the linear regression of the plot log $(F_0 - F)/F$ versus log [Q].

3. Results and discussion

3.1. Crystal structure

The Ag–atd compound crystallized in the monoclinic crystal system, *C2/c* space group, while Ag–mtn crystallized in the orthorhombic crystal system, *Aea*2 space group. The crystal structures, shown in Fig. 2, confirm the proposed compositions of the $[Ag(C_{10}H_{17}N)_2]NO_3$ and $[Ag(C_{12}H_{21}N)_2]NO_3{\cdot}H_2O$ formulas, where two amantadine or memantine molecules coordinate to silver(I) by the nitrogen atom of the amino group and nitrate as a counterion.

The Ag1—N1 bond length is 2.124 (2) Å in Ag–atd, while Ag–mtn has longer Ag1—N1 and Ag1—N2 bonds of 2.160 (2) and 2.163 (2), respectively. These values are consistent with the average of 2.14 (7) for Ag—N_{amine} bond lengths in linear geometry (N—Ag—N angles varying from 170° to 180°) found in the CSD [23]. While Ag–atd has a perfect linear geometry, Ag–mtn has a N1—Ag1—N2 bond angle of 173.4 (1)°. The geometry of the Ag–atd and Ag–mtn complexes can be compared to the one of $[Ag(NH_3)_2]^+$ complex cation, which itself presents varied N—Ag—N bond angles and lengths depending on the crystal structure [34,35].

The different orientations of the ligands in each structure proves that amantadine and memantine are free to rotate around the Ag—N bond in solution, leading to different conformations as a result of packing effects in the solid state when the compounds crystallize.

Although no other crystal structures of silver(I)–amantadine or memantine compounds were found in the database, complexes with iminoadamantane ligands have been reported. These compounds have the amino group condensed with an aldehyde, forming the imine. The silver(I) complex with two molecules of 2-(quinonyl)iminoadamantane displays a distorted tetrahedral geometry [17], whereas the complex with two 2,6-(pyridyl)iminodiadamantane ligands presents a distorted trigonal bipyramidal coordination sphere [36].

The main intermolecular interactions present in the crystal structures of Ag–atd and Ag–mtn are the hydrogen bonds between the nitrate anion and the amino groups of the aminoadamantane ligands. In the Ag–mtn crystal structure, the water molecule is also involved in the hydrogen bonding scheme.

3.2. Infrared (IR) absorption spectroscopy

The infrared (IR) spectra of the complexes and ligands are shown at the Supplementary material, Fig. S1. The bands between 2914 and 2837 cm^{-1} can be attributed to the ν(CH) and $\nu(CH_2)$ stretches of the adamantine cage [12]. The broadening of the bands of the ligands in this region (Fig. S1b and S1d), may be due to the overlap with bands related to the stretching of the amino group $\nu(NH_3^+)$ [37]. A band at 2070 cm^{-1} in the spectrum of atdH and 2053 cm^{-1}in the spectrum of mtnH were attributed to a combination of the

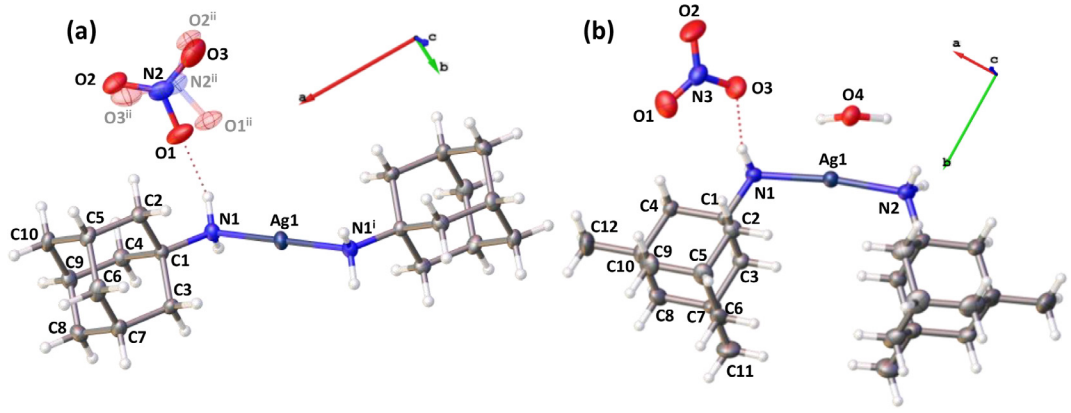

Fig. 2. Molecular view of compounds (a) Ag–atd and (b) Ag–mtn. Displacement ellipsoids are drawn at the 50% probability level. The disorder of the nitrate group of Ag–atd is represented by translucent ellipsoids. Disordered water molecules in Ag–mtn are not shown. Only one of the mtn ligands in Ag–mtn is labeled and the hydrogen atoms were not labeled, for clarity. Symmetry codes: (i) $-x+1, -y+2, -z+1$; (ii) $-x+1, y, -z+1/2$.

asymmetrical bending vibration and the torsional oscillation of the NH_3^+ group [37]. The absence of this band in the IR spectrum of the Ag–atd and Ag–mtn complexes (Fig. S1a and S1c) indicates the loss of the hydrogen atom of the R—NH_3^+ group after the conversion of atdH and mtnH to neutral forms. In addition, the presence of two well resolved bands at 3257 cm^{-1} and 3147 cm^{-1} in the spectrum of the Ag–atd complex, and at 3270 and 3154 cm^{-1} in the spectrum of the Ag–mtn complex corresponds to the asymmetric and symmetric (NH_2) stretching modes of the coordinated amino group [38], thus confirming coordination of atd or mtn to Ag(I) by the NH_2 group as already observed in the structures determined by single-crystal X-ray diffraction data.

According to the literature, free nitrate ion exhibits a strong absorption band of ν(N—O) stretching in the range 1389–1259 cm^{-1} [38,39]. As observed in Fig. S1a and S1c, the presence of a strong absorption band at 1343 and at 1321 cm^{-1}, respectively, confirms the presence of uncoordinated NO_3^- in the Ag–atd and Ag–mtn composition. The band at 3562 cm^{-1} in the spectrum of Ag–mtn confirms the presence of water in the composition of the complex. The vibration modes found to Ag–atd complex were similar of the obtained by Jeremić et al. for the $[Ag(1\text{-}AdNH_2)_2]NO_3 \cdot 0.5CH_3OH$ complex [18].

3.3. Computational simulations

To further understand the electronic structure of the metal complex with amantadine and memantine, simulations at DFT level were performed for the complexes $[Ag(atd)_2]^+$ and $[Ag(mtn)_2]^+$. In this study, the counter ion and hydration water of the system were not simulated. Fig. S2a shows the optimized structures with the ratio 2:1 ligand:silver and Fig. S2b the structures obtained experimentally from the crystal structures. The simulation results are consistent with the crystal structures when considering the N—Ag—N angle. While the N—Ag—N binding angle for the complex $[Ag(atd)_2]^+$ is 177.9°, the results found for $[Ag(mtn)_2]^+$ show that the complex has an angle of 173.7°.

The structural parameters, bond length and vibrational frequencies for the complexes are represented in Table 1. Only the vibrational frequencies of the atoms directly attached to the metal were considered for analysis. The bond length of the N—Ag bond found theoretically for $[Ag(atd)_2]^+$ was 2.187 Å and experimentally 2.124 Å. For $[Ag(mtn)_2]^+$ the theoretical bond length was 2.191 Å and the experimental one of 2.163 Å. The results also show that the theoretical data are similar to those of the crystal for other bond lengths of the complex, as presented in Table 1.

3.3.1. Frontier molecular orbitals

The frontier molecular orbitals (FMO) are of great importance because, based on their location, it is possible to perform qualitative and quantitative analyses of the possibility of a reaction occur [40]. The HOMO, LUMO and the energy gap can also generate information about the kinetic stability and chemical reactivity. Different applications of FMOs can be found in literature, such as pericyclic reactions, organic and inorganic complexes, acid and base behavior, among others [40–46]. The HOMO and LUMO orbitals and the energy gap were calculated and are presented in Figs. 3 and 4. The results show the same trends for the structures and indicate that the HOMO orbital for the ligands is mainly localized on the NH_2 group and the LUMO on the carbon atoms. For the complexes, the HOMO is mainly localized on the ligand carbon atoms and the LUMO is located on the Ag—N bond. The energy gap found for the free atd and the Ag–atd complex (ΔE = 10.20 eV and 10.10 eV), Fig. 3, are similar to the Ag–mtn results (ΔE = 10.14 eV and 9.82 eV), Fig. 4. The smaller the energy gap the more reactive the molecule is. Comparing the complexes, it is possible to suggest that Ag–mtn is slightly more reactive than Ag–atd.

3.4. Thermal analysis

The DTA and TGA curves for the silver complexes are shown in the Supplementary Material, Fig. S3. According to the experimental data, the Ag–atd compound starts to decompose at 100 °C. For Ag–mtn there is a mass loss of 4.2% above 100 °C, which is attributed to the loss of one water molecule. There are weight variations of 62.4% and 67.3% from 100 to 260 °C for Ag–atd and Ag–mtn, respectively, which correspond to the loss of two atd or mtn ligands. From 260 °C to 700 °C there were mass losses of 14.8% and 9.0% for Ag–atd and Ag–mtn, attributed to the loss of the nitrate ion. The DTA curve for Ag–atd complex exhibits a defined exothermic peak centered at 241 °C and another exothermic broad one with a maximum at 513 °C, which are consistent with the loss of the molecules of the ligand and the nitrate ion. For the Ag–mtn complex, the DTA curve shows a defined exothermic peak centered at 247 °C and another broad exothermic one centered at 388 °C, which can also be attributed to the loss of the ligand molecules and the nitrate ion as observed for the Ag–atd complex. An endothermic peak with the maximum at 140 °C is also observed for the Ag–mtn complex. This peak can be attributed to the loss of the water molecule present in the composition of the complex. At 700 °C the final residues corresponding to 22.8% for Ag–atd and 19.5% for Ag–mtn (Calcd 22.8% and 19.7%, respectively) are consistent with the formation of metallic silver. The experimental thermogravimetric data reinforces the 1:2 metal/ligand composition of the compounds and the presence of a water molecule in Ag–mtn, as verified by elemental analyses and infrared spectroscopy.

3.5. Mass spectrometric measurements

The silver complexes were analyzed by ESI(+)-QTOF-MS and the spectra are presented in the Supplementary material, Fig. S4, while the isotopic patterns (experimental and calculated) for the ions

Table 1
Experimental and theoretical bond lengths (in Å) and vibrational frequencies (in cm^{-1}) for the $[Ag(atd)_2]^+$ and $[Ag(mtn)_2]^+$ complexes.

	Complexes			
	$[Ag(atd)_2]^+$		$[Ag(mtn)_2]^+$	
Bonds	Theoretical (Å)	Experimental (Å)	Theoretical	Experimental
C—N	1.494	1.481	1.495	1.485
N—Ag	2.187	2.124	2.191	2.161
Vibration modes	Theoretical cm^{-1}	Experimental cm^{-1}	Theoretical	Experimental
ν_{as}(N—H)	3578	3258	3585	3270
ν_s(N—H)	3506	3147	3512	3154
δ(H—N—H)	1658	1589	1655	1596
ν(Ag—N)	510	–	521	–

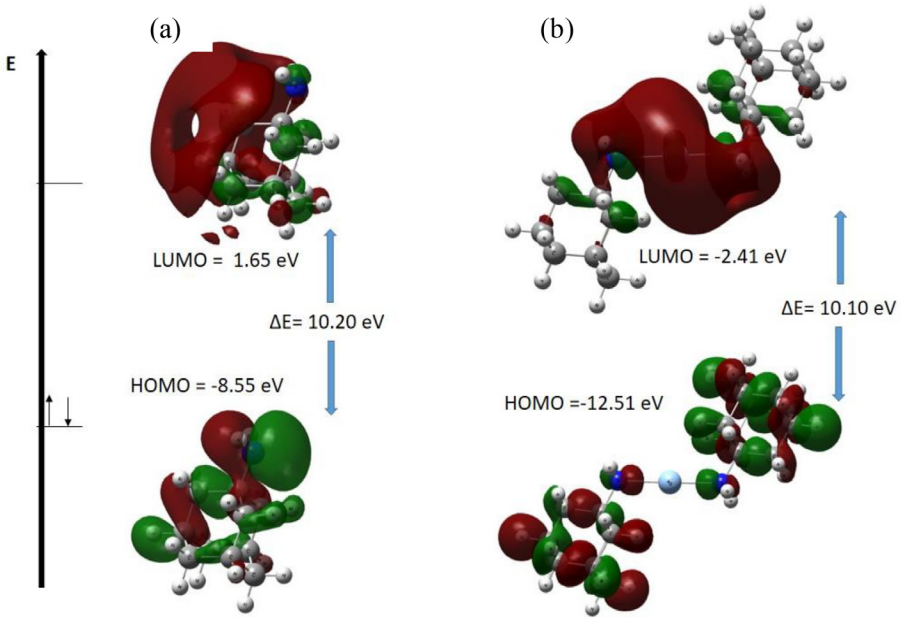

Fig. 3. HOMO, LUMO and gap for: (a) atd and (b) $[Ag(atd)_2]^+$.

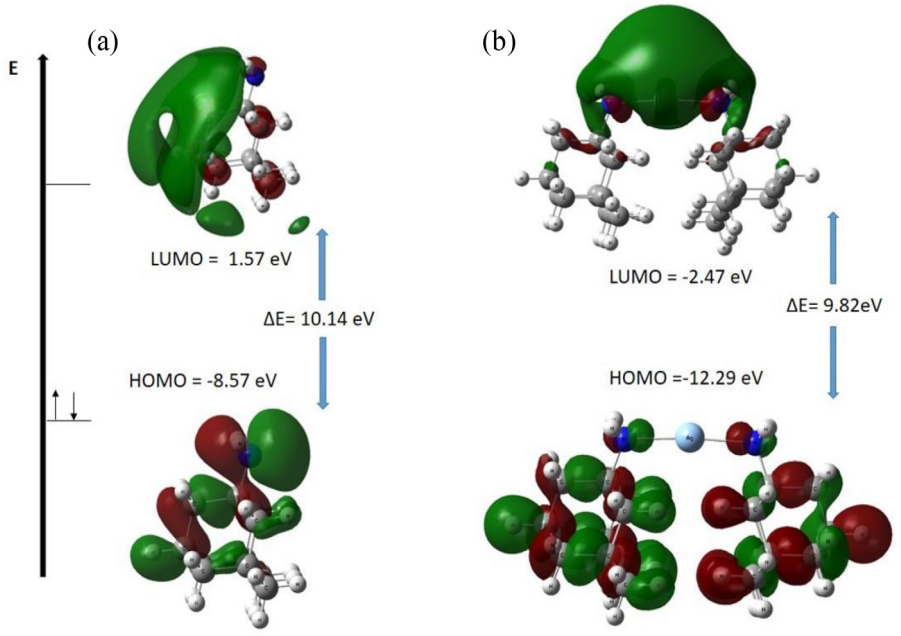

Fig. 4. HOMO, LUMO and gap for: (a) mtn and (b) $[Ag(mtn)_2]^+$.

corresponding to the expected $[AgL_2]^+$ compositions are presented in the Supplementary material, Fig. S5.

For Ag–atd, the signal observed at *m/z* 152.1512 was attributed to the $[(C_{10}H_{17}N)+H^+]$ ion, corresponding to the protonated ligand and the signal at *m/z* 409.1615 was assigned to the $[Ag(C_{10}H_{17}N)_2]^+$ ion, confirming the 1:2 metal/ligand composition. Interestingly, the mass spectrum of Ag–mtn has only one set of intense peaks at *m/z* 465.2338, corresponding to the $[Ag(C_{12}H_{21}N)_2]^+$ ion. Only for Ag–atd, peaks corresponding to atd clusters with nitric acid were observed at *m/z* 366.2743, *m/z* 580.3838 and *m/z* 794.5087. These peaks correspond to $[(C_{10}H_{17}N)_2(HNO_3)+H^+]^+$, $[(C_{10}H_{17}N)_3(HNO_3)_2+H^+]^+$ and $[(C_{10}H_{17}N)_4(HNO_3)_3+H^+]^+$ amine–nitric acid clusters, as recently reported [47] and consistent with the acidic conditions used for the experiments.

3.6. NMR spectroscopic measurements

Solution state ^1H NMR spectra of the silver complexes and of the corresponding ligands (Fig. 5) were obtained in deuterated DMSO-d_6. The spectra of the complexes were analyzed by comparison with the spectra of the corresponding ligands in order to verify if coordination of atd and mtn to Ag(I) is maintained in this solvent. The atom numbering schemes are given in Fig. 5, while signal attributions are presented in Table 2.

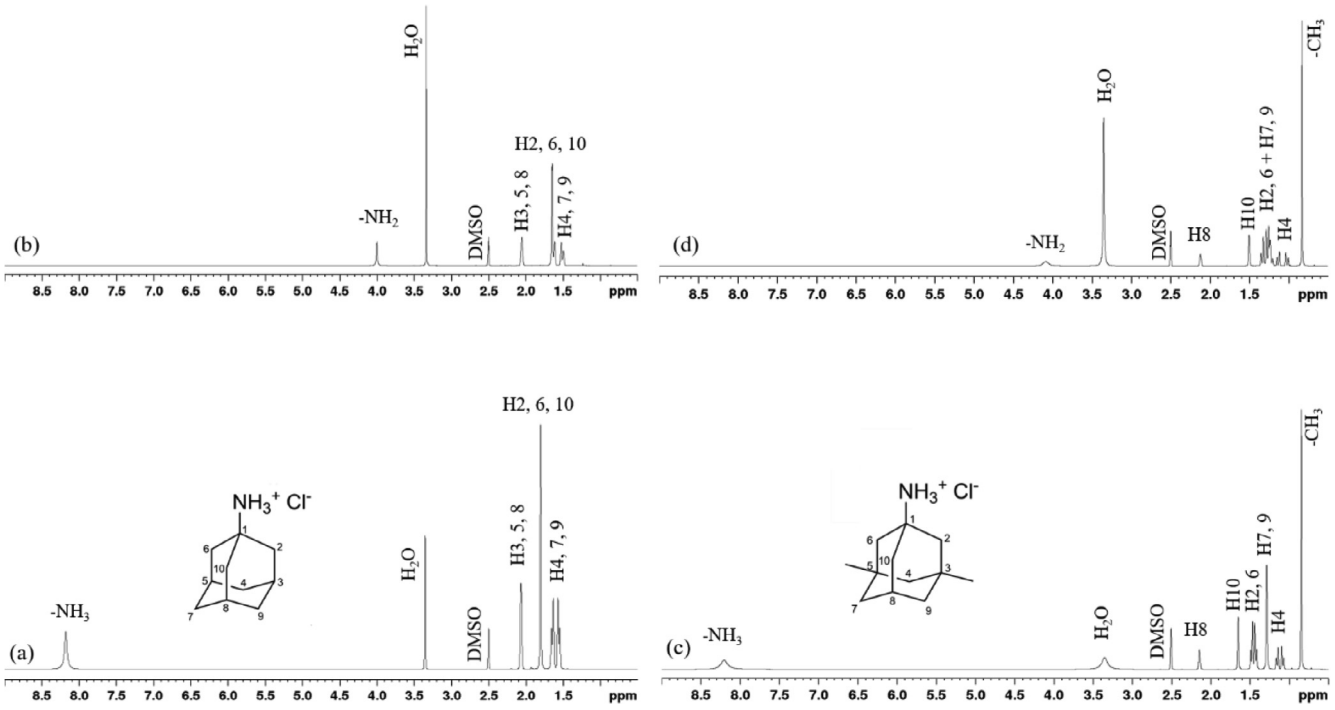

Fig. 5. ^{1}H NMR spectra of (a) atdH, (b) Ag–atd, (c) mtnH and (d) Ag–mtn. The spectra of the protonated ligands and of the silver complexes were recorded in DMSO-d_6.

Table 2
^{1}H NMR assignments and chemical shifts (ppm) for atdH, Ag–atd, mtnH and Ag–mtn. For hydrogen atoms numbering, see Fig. 5.

Assignment	Integral	atdH	Ag–atd	Assignment	Integral	mtnH	Ag–mtn
—NH_3^+/—NH_2	3	8.18	4.00	—NH_3^+/—NH_2	3	8.20	4.09
H4, H7, H9	6	1.60	1.57	H2, H6	4	1.45	1.32
H2, H6, H10	6	1.80	1.65	H4	2	1.12	1.07
H3, H5, H8	3	2.06	2.05	H7, H9	4	1.29	1.23
				H8	1	2.15	2.12
				H10	2	1.65	1.5
				—CH_3	6	0.85	0.84

The ^{1}H NMR spectra of atdH and Ag–atd present differences in chemical shifts, which may be attributed to coordination. The most remarkable shift corresponds to the signal from the hydrogen atoms of the —NH_3^+ group of atdH, seen at 8.18 ppm, which are observed at 4.00 ppm in the Ag–atd spectrum when coordinated to silver as —NH_2.

The presence of two additional methyl groups in the structure of mtnH when compared to atdH leads to a distinct ^{1}H NMR spectra. However, the same changes in the chemical shifts occur when comparing mtnH and Ag–mtn, also suggesting that coordination of the ligand to Ag(I) is maintained in solution.

The {^{15}N,^{1}H} NMR HMBC experiments were performed to see direct changes on the electronic density of the nitrogen atom after coordination to silver. The 2D correlation maps are given in the Supplementary material, Fig. S6.

The nitrogen atoms of the R—NH_3^+ groups of atdH and mtnH are observed at 62.0 and 60.6 ppm, respectively, while for their corresponding complexes, the signals were found at 51.6 ppm and 49.7 ppm. The variation $\Delta\delta$ (δ complex $-$ δ ligand) of -10.4 and -10.9, respectively, attest for the fact that coordination of atd and mtn to silver(I) by the N atom of the NH_2 group is retained in solution. Finally, in order to see if the complexes undergo any significant ligand replacement by the solvent (DMSO-d_6), the ^{1}H NMR spectra of the compounds were recorded with time, for a period of 24 h. The sets of spectra for Ag–atd and Ag–mtn are presented in Supplementary material, Fig. S7. No apparent ligand replacement in DMSO-d_6 is observed during the evaluated time period.

3.7. Minimum inhibitory concentration (MIC)

The antibacterial activities of the Ag–atd and Ag–mtn complexes and its precursors against Gram-negative and Gram-positive microorganisms were evaluated by the MIC assay. Ampicillin was used as a control antibacterial drug for this experiment. The results are shown in Table 3.

The bacterial strains were resistant to the ligand atdH in the considered experimental conditions while mtnH presented activity against *S. aureus* and *P. aeruginosa*. Although mtnH was active only at a high concentration, this antibacterial activity had never been reported for this molecule.

The MIC values of Ag–atd, Ag–mtn and $AgNO_3$ against the tested bacterial strains revealed activity on the micromolar range. The Ag–atd complex was more active than Ag–mtn over all tested bacterial strains. Ag–atd was also more active than $AgNO_3$, especially against Gram-positive bacterial strains, which indicates this compound may have a mechanism of action that is not solely related to the silver ion. The fact that $AgNO_3$ has a pronounced antibacterial activity by itself is well reported in the literature. Nevertheless, it is also known that this silver salt is toxic to human tissues and

Table 3
Comparison between minimum inhibitory concentration values of Ag–atd, Ag–mtn, atdH, mtnH and $AgNO_3$ against the four bacterial strains tested.

Compounds	Minimum inhibitory concentration (mmol L^{-1})			
	S. aureus ATCC – 25923	*B. cereus* ATCC – 14579	*E. coli* ATCC – 25922	*P. aeruginosa* ATCC – 27853
atdH	R	R	R	R
mtnH	9.27	R	R	9.27
Ag–atd	16.5×10^{-3}	16.5×10^{-3}	16.5×10^{-3}	16.5×10^{-3}
Ag–mtn	114.0×10^{-3}	57.2×10^{-3}	57.2×10^{-3}	57.2×10^{-3}
$AgNO_3$	46.0×10^{-3}	46.0×10^{-3}	23.0×10^{-3}	23.0×10^{-3}
Ampicillin	28.6×10^{-3}	28.6×10^{-3}	1.8×10^{-3}	7.1×10^{-3}

R = Resistant.

presents low selectivity [48]. Given the low MIC values of Ag–atd and Ag–mtn against the bacterial strains tested, further assays should be performed to evaluate the extent of their antibacterial properties, as well as to determine the toxicity of these complexes to human cells.

Besides that, the complexes showed better activity against the Gram-negative microorganisms *P. aeruginosa* and *E. coli* when compared to a Au(I)–rimantadine complex previously reported by our research group [37]. The results are also consistent with the formerly reported data on the antibacterial activity of the $[Ag(1\text{-}AdNH_2)_2]NO_3{\cdot}0.5CH_3OH$ complex against *S. aureus* and *E. coli* [18].

3.8. Agarose gel electrophoresis

Studies about interaction of the compounds with biomolecules is generally performed to investigate its possible molecular targets. In this case, the capacity of the aminoadamantane ligands and their corresponding silver complexes to alter the conformation of plasmid DNA was monitored by agarose gel electrophoresis assay. Cisplatin in different concentrations was used as positive control. The results are presented in Fig. 6.

The plasmid DNA is separated by electrophoresis in different bands which are divided due to three main conformations as shown in Fig. 6: open circular form (OC), linear form (LF) and super coiled form (SC) [49,50]. These plasmid conformations are separated in a way where the more condensated forms can migrate further in the gel, while the open forms migrate less. When the migration profile of the DNA bands is altered, there is evidence of interaction with the compounds tested. Fig. 6 showed that cisplatin, which is known by its ability to for covalent adducts with DNA [51], presents considerable alteration in the DNA bands in the two concentration evaluated, while $AgNO_3$, the aminoadamantane ligands and their silver complexes do not covalently interact with DNA under the considered experimental conditions.

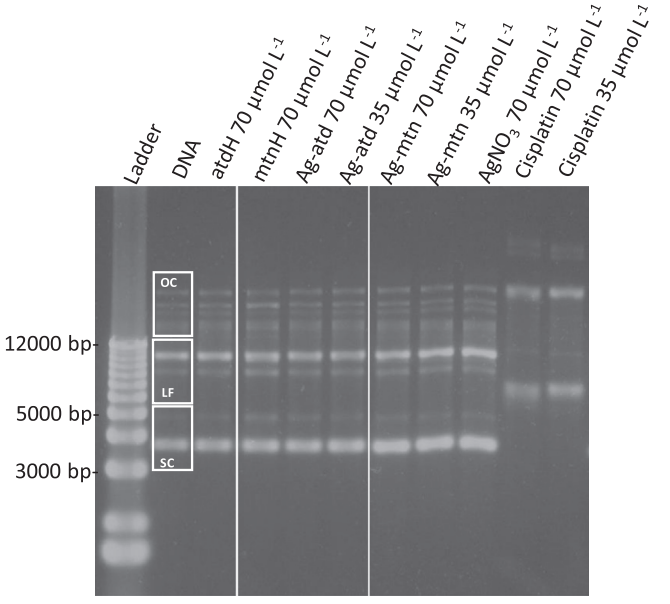

Fig. 6. Agarose gel electrophoresis of the circular DNA in the presence of atdH, mtnH, Ag–atd, Ag–mtn, $AgNO_3$ and cisplatin at different concentrations. OC = Open circular, LF = linear form and SC = supercoiled forms of the pGEX-4T1 plasmid.

3.9. Studies of interaction with DNA by fluorescence spectroscopy

Fluorescence spectroscopy was used to further evaluate the interaction between the compounds and DNA by competitive binding with the SYBr Green fluorophore, Fig. 7. When this dye interacts with DNA (dye/base pair ratios above 0.15) [52], a fluorescence signal rises due to minor groove binding. In this case, if the compounds of interest can disrupt the DNA–SG interaction, fluorescence quenching occurs.

According to the results presented in Fig. 7, there is only a small interaction of compounds evaluated with CT-DNA, with the greatest quenching fluorescence resulting from atdH and Ag–atd. The presence of the methyl groups in mtnH seems to have lowered the affinity of this ligand and its corresponding silver complex with DNA. The small fluorescence quenching indicates a non-covalent mode of interaction with DNA. Additionally, the positive charge on the ligands and complexes and their ability to form hydrogen bonds by the NH_2 group suggest that the interaction is of electrostatic nature or by groove binding [53].

3.10. Studies of interaction with BSA by fluorescence spectroscopy

Serum albumins are present in highest concentration in blood plasma and acts such as a transporter of exogenous and

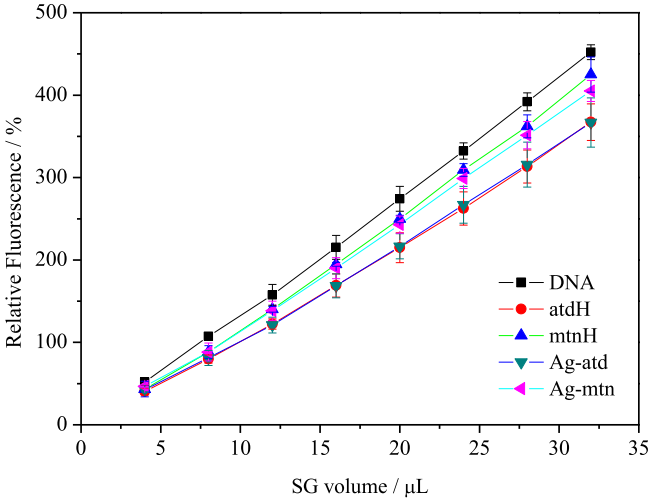

Fig. 7. Relative fluorescence intensities of SG in the presence of free DNA and DNA incubated with atdH, mtnH, Ag–atd and Ag–mtn in the ratio (compound/DNA) 0.3.

Table 4
Stern–Volmer constant (K_{sv}), binding constant (K_b), and percentage of fluorescence intensity decrease for the interaction of Ag–atd, Ag–mtn and $AgNO_3$ with BSA.

Compounds	K_{sv} (L mol^{-1})	K_b (L mol^{-1})	Decrease (%)
Ag–atd	4.4×10^3	2.04×10^2	13.0%
Ag–mtn	6.6×10^3	1.17×10^3	17.5%
$AgNO_3$	5.4×10^3	2.07×10^2	15.7%

endogenous substances in the organisms [33]. Fluorescence spectroscopy was used to evaluate the interaction of the complexes with the protein through tryptophan fluorescence quenching, the main amino acid residue responsible for BSA fluorescence [54]. The effects of the Ag–atd and Ag–mtn complexes, on the BSA fluorescence intensity are shown in Fig. S8.

The spectra obtained by titration of Ag–atd and Ag–mtn in BSA solution showed 13.0% and 17.5%, respectively, of fluorescence quenching of BSA at the highest tested concentration ([complexes] = 30.0 μmol L^{-1}), similar to the fluorescence quenching obtained to $AgNO_3$ (15.7%) at the same concentration, while atdH, mtnH and the solvent did not present any considerable quenching in the BSA fluorescence. The linearized fluorescence data (at 347 nm) of the protein in the presence of the Ag–atd and Ag–mtn complexes are presented in Supplementary material, Fig. S9. A comparison between the K_{sv}, K_q and K_b values of the complexes, $AgNO_3$ and the percentage of decrease of the initial fluorescence intensity of BSA are shown in Table 4.

The binding constant values, K_b, are not as high as the values described in the literature for other silver(I) complexes [55,56], indicating the interaction of Ag–atd and Ag–mtn with BSA is weaker than those previously reported. The similarity of the results obtained for the complexes and $AgNO_3$ suggests influence of the concentration of Ag^+ ions on the fluorescence-quenching of BSA [57].

4. Conclusion

Silver(I) complexes with amantadine and memantine with coordination formula $[Ag(C_{10}H_{17}N)_2]NO_3$ and $[Ag(C_{12}H_{21}N)_2]NO_3 \cdot H_2O$ were obtained and their compositions were determined by elemental, thermal and mass spectrometric analyses. The structures of the complexes were solved by single crystal X-ray diffractometry, where each molecule of ligand coordinates to silver(I) by the nitrogen atom of the NH_2 group in a linear geometry. The electronic and vibrational properties of the synthesized molecule were further studied by FTIR spectroscopy and DFT. The complexes exhibited antibacterial activity over Gram-positive and Gram-negative microorganisms with MIC values in the micromolar range. The agarose gel electrophoresis assays showed that the complexes do not interact covalently with plasmid DNA, but competitive binding experiments showed that electrostatic or groove interactions may occur. Fluorescence spectroscopic studies revealed 13.0% and 15.7% of decrease in the fluorescence intensity of bovine serum albumin (BSA) in the presence of the Ag–atd and Ag–mtn complexes, respectively, which indicates that such compounds interact weakly with this biomolecule.

Acknowledgements

This study was supported by grants from the Brazilian Agencies FAPESP (São Paulo Research Foundation), grants 2013/22127-2, 2014/50906-9, 2015/20882-3, 2017/25995-6, 2018/12062-4 and 2018/12590-0, CNPq (National Council for Scientific and Technological Development, grant #407012/2018-4 and 164658/2018-1). This study was also financed in part by the Coordenação de Aperfeiçoamento de Pessoal de Nível Superior – Brazil (CAPES) – Finance Code 001.

Appendix A. Supplementary data

CCDC 1908792 and 1913280 contain the supplementary crystallographic data. These data can be obtained free of charge via http://www.ccdc.cam.ac.uk/conts/retrieving.html, or from the Cambridge Crystallographic Data Centre, 12 Union Road, Cambridge CB2 1EZ, UK; fax: (+44) 1223-336-033; or e-mail: deposit@ccdc.cam.ac.uk. Supplementary data to this article can be found online at https://doi.org/10.1016/j.poly.2019.114116.

References

[1] J.H. Bormio Nunes, R.E.F. de Paiva, A. Cuin, W.R. Lustri, P.P. Corbi, Silver complexes with sulfathiazole and sulfamethoxazole: synthesis, spectroscopic characterization, crystal structure and antibacterial assays, Polyhedron 85 (2015) 437, https://doi.org/10.1016/j.poly.2014.09.010.
[2] A.F. Santos, I.P. Ferreira, C.B. Pinheiro, J.A. Takahashi, L.R. Teixeira, H. Beraldo, Silver(I) complexes with 2,6-diacetylpyridine-bis (benzoylhydrazones): antifungal activity and interaction with DNA, Polyhedron 138 (2017) 270, https://doi.org/10.1016/j.poly.2017.09.019.
[3] J.H.B. Nunes, F.R.G. Bergamini, W.R. Lustri, P.P. de Paiva, A.L.T.G. Ruiz, J.E. de Carvalho, P.P. Corbi, Synthesis, characterization and in vitro biological assays of a silver(I) complex with 5-fluorouracil: a strategy to overcome multidrug resistant tumor cells, J. Fluor. Chem. 195 (2017) 93, https://doi.org/10.1016/j.jfluchem.2017.01.016.
[4] M. Cavicchioli, A.C. Massabni, T.A. Heinrich, C.M. Costa-Neto, E.P. Abrão, B.A.L. Fonseca, E.E. Castellano, P.P. Corbi, W.R. Lustri, C.Q.F. Leite, Pt(II) and Ag(I) complexes with acesulfame: crystal structure and a study of their antitumoral, antimicrobial and antiviral activities, J. Inorg. Biochem. 104 (2010) 533–540, https://doi.org/10.1016/j.jinorgbio.2010.01.004.
[5] P.C. Zachariadis, S.K. Hadjikakou, N. Hadjiliadis, S. Skoulika, A. Michaelides, J. Balzarini, E. De Clercq, Synthesis, characterization and in vitro study of the cytostatic and antiviral activity of new polymeric silver(I) complexes with ribbon structures derived from the conjugated heterocyclic thioamide 2-mercapto-3,4,5,6-tetra-hydropyrimidine, Eur. J. Inorg. Chem. 2004 (2004) 1420–1426, https://doi.org/10.1002/ejic.200300672.
[6] I. Sainis, C.N. Banti, A.M. Owczarzak, L. Kyros, N. Kourkoumelis, M. Kubicki, S.K. Hadjikakou, New antibacterial, non-genotoxic materials, derived from the functionalization of the anti-thyroid drug methimazole with silver ions, J. Inorg. Biochem. 160 (2016) 114–124, https://doi.org/10.1016/j.jinorgbio.2015.12.013.
[7] E. Alberti, M. Zampakou, D. Donghi, Covalent and non-covalent binding of metal complexes to RNA, J. Inorg. Biochem. 163 (2016) 278–291, https://doi.org/10.1016/j.jinorgbio.2016.04.021.
[8] C.M. Manzano, F.R.G. Bergamini, W.R. Lustri, A.L.T.G. Ruiz, E.C.S. de Oliveira, M. A. Ribeiro, A.L.B. Formiga, P.P. Corbi, Pt(II) and Pd(II) complexes with ibuprofen hydrazide: characterization, theoretical calculations, antibacterial and antitumor assays and studies of interaction with CT-DNA, J. Mol. Struct. 1154 (2018) 469–479, https://doi.org/10.1016/j.molstruc.2017.10.072.
[9] A.T.M. Fiori, D.H. Nakahata, A. Cuin, W.R. Lustri, P.P. Corbi, Synthesis, crystallographic studies, high resolution mass spectrometric analyses and antibacterial assays of silver(I) complexes with sulfisoxazole and sulfadimethoxine, Polyhedron 121 (2017) 172–179, https://doi.org/10.1016/j.poly.2016.09.046.
[10] D.H. Nakahata, M.A. Ribeiro, P.P. Corbi, D. Machado, M. Lancellotti, W.R. Lustri, A.M. da Costa Ferreira, A.L.B. Formiga, Synthesis, characterization and preliminary antimicrobial assays of copper(II) complexes with 2-(imidazole-2-yl)heteroaryl ligands, Inorg. Chim. Acta 458 (2017) 224–232, https://doi.org/10.1016/j.ica.2017.01.015.
[11] C. Scholtissek, G. Quack, H.D. Klenk, R.G. Webster, How to overcome resistance of influenza A viruses against adamantane derivatives, Antiviral Res. 37 (1998) 83–95. http://www.ncbi.nlm.nih.gov/pubmed/9588841.
[12] J.C. Garcia, J.F. Justo, W.V.M. Machado, L.V.C. Assali, Structural, electronic, and vibrational properties of amino-adamantane and rimantadine isomers, J. Phys. Chem. A 114 (2010) 11977–11983, https://doi.org/10.1021/jp107496b.
[13] J. Folch, O. Busquets, M. Ettcheto, E. Sánchez-López, R.D. Castro-Torres, E. Verdaguer, M.L. Garcia, J. Olloquequi, G. Casadesús, C. Beas-Zarate, C. Pelegri, J. Vilaplana, C. Auladell, A. Camins, Memantine for the treatment of dementia: a review on its current and future applications, J. Alzheimers Dis. 62 (2018) 1223–1240, https://doi.org/10.3233/JAD-170672.
[14] R.J. van Marum, Update on the use of memantine in Alzheimer's disease, Neuropsychiatr. Dis. Treat. 5 (2009) 237–247. http://www.ncbi.nlm.nih.gov/pubmed/19557118.
[15] R.A. Bright, D.K. Shay, B. Shu, N.J. Cox, A.I. Klimov, Adamantane resistance among influenza A viruses isolated early during the 2005–2006 influenza season in the United States, JAMA 295 (2006) 891, https://doi.org/10.1001/jama.295.8.joc60020.

[16] Y. Li, Z. Lin, M. Zhao, M. Guo, T. Xu, C. Wang, H. Xia, B. Zhu, Reversal of H1N1 influenza virus-induced apoptosis by silver nanoparticles functionalized with amantadine, RSC Adv. 6 (2016) 89679–89686, https://doi.org/10.1039/C6RA18493F.

[17] J. Jimenez, I. Chakraborty, M. Rojas-Andrade, P.K. Mascharak, Silver complexes of ligands derived from adamantylamines: Water-soluble silver-donating compounds with antibacterial properties, J. Inorg. Biochem. 168 (2017) 13–17, https://doi.org/10.1016/j.jinorgbio.2016.12.009.

[18] D. Jeremic, M. Djordjevic, S. Miletic, L. Andjelkovic, D. Sladic, I. Brceski, Novel silver(I) compounds with 1-adamantanamine, J. Serb. Chem. Soc. 83 (2018) 699–705, https://doi.org/10.2298/JSC171114041J.

[19] G.M. Sheldrick, SHELXT – Integrated space-group and crystal-structure determination, Acta Crystallogr. A 71 (2015) 3–8, https://doi.org/10.1107/S2053273314026370.

[20] G.M. Sheldrick, Crystal structure refinement with SHELXL, Acta Crystallogr., Sect. C: Struct. Chem. 71 (2015) 3–8, https://doi.org/10.1107/S2053229614024218.

[21] O.V. Dolomanov, L.J. Bourhis, R.J. Gildea, J.A.K. Howard, H. Puschmann, OLEX2: a complete structure solution, refinement and analysis program, J. Appl. Crystallogr. 42 (2009) 339–341, https://doi.org/10.1107/S0021889808042726.

[22] C.F. Macrae, I.J. Bruno, J.A. Chisholm, P.R. Edgington, P. McCabe, E. Pidcock, L. Rodriguez-Monge, R. Taylor, J. van de Streek, P.A. Wood, MERCURY CSD 2.0 – new features for the visualization and investigation of crystal structures, J. Appl. Crystallogr. 41 (2008) 466–470, https://doi.org/10.1107/s0021889807067908.

[23] C.R. Groom, I.J. Bruno, M.P. Lightfoot, S.C. Ward, The Cambridge structural database, Acta Crystallogr. Sect. B: Struct. Sci. Cryst. Eng. Mater. 72 (2016) 171–179, https://doi.org/10.1107/S2052520616003954.

[24] I.J. Bruno, J.C. Cole, P.R. Edgington, M. Kessler, C.F. Macrae, P. McCabe, J. Pearson, R. Taylor, IUCr, New software for searching the Cambridge Structural Database and visualizing crystal structures, Acta Crystallogr. Sect. B: Struct. Sci. 58 (2002) 389–397, https://doi.org/10.1107/S0108768102003324.

[25] J. Chai, M. Head-gordon, Long-range corrected hybrid density functionals with damped atom – atom dispersion corrections, Phys. Chem. Chem. Phys. 10 (2008) 6615–6620, https://doi.org/10.1039/b810189b.

[26] R. Ditchfield, W.J. Hehre, J.A. Pople, Self-consistent molecular-orbital methods. IX. An extended Gaussian-type basis for molecular-orbital studies of organic molecules, J. Chem. Phys. 54 (1971) 724–728, https://doi.org/10.1063/1.1674902.

[27] W.J. Hehre, R. Ditchfield, J.A. Pople, Self-consistent molecular orbital methods. XII. Further extensions of Gaussian—type basis sets for use in molecular orbital studies of organic molecules, J. Chem. Phys. 56 (1972) 2257–2261, https://doi.org/10.1063/1.1677527.

[28] P.C. Hariharan, J.A. Pople, The influence of polarization functions on molecular orbital hydrogenation energies, Theor. Chim. Acta 28 (1973) 213–222, https://doi.org/10.1007/BF00533485.

[29] P.J. Hay, W.R. Wadt, Ab, initio effective core potentials for molecular calculations. Potentials for the transition metal atoms Sc to Hg, J. Chem. Phys. 82 (1985) 270–283, https://doi.org/10.1063/1.448799.

[30] M.J. Frisch, G.W. Trucks, H.B. Schlegel, G. Scuseria, M.A. Robb, J.R. Cheeseman, G. Scalmani, V. Barone, B. Mennucci, G. Petersson, H. Nakatsuji, M. Caricato, X. Li, H.P. Hratchian, A.F. Izmaylov, J. Bloino, G. Zheng, J.L. Sonnenberg, M. Hada, M. Ehara, K. Toyota, R. Fukuda, J. Hasegawa, M. Ishida, T. Nakajima, Y. Honda, O. Kitao, H. Nakai, T. Vreven, J.A. Montgomery, J.E. Peralta, F. Ogliaro, M. Bearpark, J.J. Heyd, B.E.K.N. Kudin, V.N. Staroverov, R. Kobayashi, J. Normand, K. Raghavachari, A. Rendell, J.C. Burant, S.S. Iyengar, J. Tomasi, M. Cossi, N. Rega, J.M. Millam, M. Klene, J.E. Knox, J.B. Cross, V. Bakken, C. Adamo, J. Jaramillo, R. Gomperts, R.E. Stratmann, O. Yazyev, A.J. Austin, R. Cammi, C. Pomelli, J.W. Ochterski, R.L. Martin, K. Morokuma, V.J. Zakrzewski, G.A. Voth, P. Salvador, J.J. Dannenberg, S. Dapprich, A.D. Daniels, O. Farkas, J.B. Foresman, J. V. Ortiz, J. Cioslowski, D.J. Fox, D. 0109, Revision D. 01, Gaussian, Inc., Wallingford, CT, 2009.

[31] Clinical and Laboratory Standards Institute (CLSI), Performance Standards for Antimicrobial Susceptibility Testing, 26th ed., Clinical and Laboratory Standards Institute, 950 West Valley Road, Suite 2500, Wayne, Pennsylvania 19087 USA, 2016.

[32] V. Kondaparthy, A. Shaik, K.B. Reddy, D. Das Manwal, Studies on interaction of vanadium metal complexes with bovine serum albumin – fluorometric and UV–visible spectrophotometric studies, Chem. Data Collect. 20 (2019), https://doi.org/10.1016/j.cdc.2019.100203 100203.

[33] X. Jin, Y. Yang, Y. Jiang, X. Han, X. Wan, D. Liu, X. Song, X. Chang, Synthesis, characterization and interaction with bovine serum albumin of cyclometallated Pd(II) complexes containing arylimine and salicylaldimine co-ligands, J. Organomet. Chem. 791 (2015) 24–33, https://doi.org/10.1016/j.jorganchem.2015.04.050.

[34] D. Sun, F.-J. Liu, R.-B. Huang, L.-S. Zheng, Structural diversity of Ag/3-nitrophthalate coordination polymers controlled by solvent and induction agent, CrystEngComm. 15 (2013) 1185–1193, https://doi.org/10.1039/C2CE26659H.

[35] Z.P. Deng, L.H. Huo, M.S. Li, L.W. Zhang, Z.B. Zhu, H. Zhao, S. Gao, Syntheses, structures, and luminescent properties of silver(I) complexes constructed from ortho-hydroxyl arenesulfonic acids, Cryst. Growth Des. 11 (2011) 3090–3100, https://doi.org/10.1021/cg200360e.

[36] J. Jimenez, I. Chakraborty, A.M. Del Cid, P.K. Mascharak, Five- and six-coordinated silver(I) complexes derived from 2,6-(pyridyl) iminodiadamantanes: sustained release of bioactive silver toward bacterial eradication, Inorg. Chem. 56 (2017) 4784–4787, https://doi.org/10.1021/acs.inorgchem.7b00621.

[37] S.F. Sucena, R.E.F. Paiva, C. Abbehausen, I.B. Mattos, M. Lancellotti, A.L.B. Formiga, P.P. Corbi, Chemical, spectroscopic characterization, DFT studies and antibacterial activities in vitro of a new gold(I) complex with rimantadine, Spectrochim. Acta – Part A: Mol. Biomol. Spectrosc. 89 (2012) 114–118, https://doi.org/10.1016/j.saa.2011.12.043.

[38] S.O. Podunavac-kuzmanovi, D.M. Cvetkovi, L.S. Vojinovi, Synthesis, physico-chemical characterization and biological activity of 2-aminobenzimidazole complexes with different metal ions, Acta Period. Technol. 280 (2004) 239–246.

[39] Y.S. Mary, H.T. Varghese, C.Y. Panicker, T. Ertan, I. Yildiz, O. Temiz-Arpaci, Vibrational spectroscopic studies and ab initio calculations of 5-nitro-2-(p-fluorophenyl)benzoxazole, Spectrochim. Acta, Part A: Mol. Biomol. Spectrosc. 71 (2008) 566–571, https://doi.org/10.1016/j.saa.2007.12.041.

[40] M. Sheikhi, S. Shahab, M. Khaleghian, F.H. Hajikolaee, I. Balakhanava, R. Alnajjar, Adsorption properties of the molecule resveratrol on CNT(8,0–10) nanotube: geometry optimization, molecular structure, spectroscopic (NMR, UV/Vis, excited state), FMO, MEP and HOMO-LUMO investigations, J. Mol. Struct. 1160 (2018) 479–487, https://doi.org/10.1016/j.molstruc.2018.01.005.

[41] M. Sheikhi, S. Shahab, M. Khaleghian, R. Kumar, Interaction between new anti-cancer drug syndros and CNT(6,6-6) nanotube for medical applications: geometry optimization, molecular structure, spectroscopic (NMR, UV/Vis, excited state), FMO, MEP and HOMO-LUMO investigation, Appl. Surf. Sci. 434 (2018) 504–513, https://doi.org/10.1016/j.apsusc.2017.10.154.

[42] D.H. Pereira, F.A. La Porta, R.T. Santiago, D.R. Garcia, T.C. Ramalho, New perspectives on the role of frontier molecular orbitals in the study of chemical reactivity: a review, Rev. Virt. Quím. 8 (2016) 425–453, https://doi.org/10.5935/1984-6835.20160032.

[43] H. Fujimoto, Y. Mizutani, K. Iwase, An aspect of substituents and peripheral structures in chemical reactivities of molecules, J. Phys. Chem. 90 (1986) 2768–2772, https://doi.org/10.1021/j100403a042.

[44] H. Hirao, T. Ohwada, Theoretical study of reactivities in electrophilic aromatic substitution reactions: reactive hybrid orbital analysis, J. Phys. Chem. A 107 (2003) 2875–2881, https://doi.org/10.1021/jp027330l.

[45] R. Vianello, Z.B. Maksić, Triadic analysis of substituent effects—gas-phase acidity of para-substituted phenols, Tetrahedron 62 (2006) 3402–3411, https://doi.org/10.1016/j.tet.2006.01.049.

[46] R.R. da Silva, J.M. Santos, T.C. Ramalho, J.D. Figueroa-Villar, Concerning the FERMO concept and Pearson's hard and soft acid-base principle, J. Braz. Chem. Soc. 17 (2006) 223–226, https://doi.org/10.1590/S0103-50532006000200002.

[47] M. Kumar, H. Li, X. Zhang, X.C. Zeng, J.S. Francisco, Nitric acid-amine chemistry in the gas phase and at the air-water interface, J. Am. Chem. Soc. 140 (2018) 6456–6466, https://doi.org/10.1021/jacs.8b03300.

[48] B.S. Atiyeh, M. Costagliola, S.N. Hayek, S.A. Dibo, Effect of silver on burn wound infection control and healing: review of the literature, Burns 33 (2007) 139–148, https://doi.org/10.1016/j.burns.2006.06.010.

[49] M.J. Molloy, Effective and robust plasmid topology analysis and the subsequent characterization of the plasmid isoforms thereby observed, Nucleic Acids Res. 32 (2004) 129, https://doi.org/10.1093/nar/gnh124.

[50] M.S. Levy, Quantitation of supercoiled circular content in plasmid DNA solutions using a fluorescence-based method, Nucleic Acids Res. 28 (2000) 57, https://doi.org/10.1093/nar/28.12.e57.

[51] A.C. Komor, J.K. Barton, The path for metal complexes to a DNA target, Chem. Commun. 49 (2013) 3617, https://doi.org/10.1039/c3cc00177f.

[52] M.E. Bravo-Gómez, C. Campero-Peredo, D. García-Conde, M.J. Mosqueira-Santillán, J. Serment-Guerrero, L. Ruiz-Azuara, DNA-binding mode of antitumoral copper compounds (Casiopeinas®) and analysis of its biological meaning, Polyhedron 102 (2015) 530–538, https://doi.org/10.1016/j.poly.2015.10.034.

[53] V. Censi, A.B. Caballero, M. Pérez-Hernández, V. Soto-Cerrato, L. Korrodi-Gregório, R. Pérez-Tomás, M.M. Dell'Anna, P. Mastrorilli, P. Gamez, DNA-binding and in vitro cytotoxic activity of platinum(II) complexes of curcumin and caffeine, J. Inorg. Biochem. 198 (2019), https://doi.org/10.1016/j.jinorgbio.2019.110749 110749.

[54] A.V. Protas, E.A. Popova, O.V. Mikolaichuk, Y.B. Porozov, A.R. Mehtiev, I. Ott, G. V. Alekseev, N.A. Kasyanenko, R.E. Trifonov, Synthesis, DNA and BSA binding of Pd(II) and Pt(II) complexes featuring tetrazolylacetic acids and their esters, Inorg. Chim. Acta 473 (2018) 133–144, https://doi.org/10.1016/j.ica.2017.12.040.

[55] N. Shahabadi, M. Maghsudi, Z. Ahmadipour, Study on the interaction of silver (I) complex with bovine serum albumin by spectroscopic techniques, Spectrochim. Acta, Part A: Mol. Biomol. Spectrosc. 92 (2012) 184–188, https://doi.org/10.1016/j.saa.2012.02.071.

[56] S. Parveen, S. Govindarajan, H. Puschmann, R. Revathi, Synthesis, crystal structure and biological studies of new hydrazone ligand, 2-(methoxycarbonyl-hydrazono)-pentanedioic acid and its silver(I) complex, Inorg. Chim. Acta 477 (2018) 66–74, https://doi.org/10.1016/j.ica.2018.02.022.

[57] X. Zhao, R. Liu, Y. Teng, X. Liu, The interaction between Ag+ and bovine serum albumin: a spectroscopic investigation, Sci. Total Environ. 409 (2011) 892–897, https://doi.org/10.1016/j.scitotenv.2010.11.004.